JOURNAL OF MATERIALS SCIENCE **34** (1999) 2821–2835

The microstructural characterization of *in situ* grown Si_3N_4 whisker-reinforced barium aluminum silicate ceramic matrix composite

F. YU, C. R. ORTIZ-LONGO, K. W. WHITE
Department of Mechanical Engineering, University of Houston, Houston, Texas 77204-4792

DAVID L. HUNN
Loral Vought Systems, Corp., P. O. Box 650003, Dallas, TX 75265-0003
E-mail: fxy5571@jetson.uh.edu

The microstructure of Barium Aluminum Silicate (BAS)/Silicon Nitride *in situ* whisker reinforced ceramic matrix composite was examined by X-ray diffraction, transmission electron microscopy, electron diffraction and energy-dispersive X-ray microanalysis. Although we cannot conclusively exclude the presence of orthorhombic BAS, hexagonal BAS and both α-Si_3N_4 and β-Si_3N_4 were identified in this material. The crystallization process of the glass phase can be taken almost to completion but a small proportion of residual glass phase is present. Both whiskerlike and equiaxed β-Si_3N_4 exist in this material.

1. Introduction

The increasing demand for high performance materials in the aerospace and other structural applications, where a combination of high temperature strength and resistance to environmental degradation are important, has led to the development of a variety of ceramic materials based on the compositions Si_3N_4, Al_2O_3 and SiC. Among these ceramic materials, silicon nitride (Si_3N_4) is one of the most promising materials for service under 1500 °C because of its strength at high temperature, good thermal stress resistance, and relatively good resistance to oxidation when compared to other high temperature structural materials (see Table I) [1–4].

In the last 18 years, two principal directions have been charted in the processing of Si_3N_4-based materials, (i) dense Si_3N_4 produced by hot-pressing sintering, or hot-isostatic processing and (ii) reaction bonded Si_3N_4 produced by reacting silicon powder compacts in a controlled N_2 atmosphere [1]. Both of these types, as with other engineering ceramics, suffer from a relatively poor fracture resistance, requiring improvements in reliability to satisfy many design criteria for practical applications. Therefore, microstructural modifications to alleviate this problem have recently been the subject of much effort in the research community.

To this end, various whisker reinforcements have been applied to engineering ceramics [5–9]. It has been shown that proper selection of whisker reinforcements could significantly increase its fracture resistance [5, 6]. However, problems associated with fabricating whisker-reinforced ceramic composites include the high cost of the whiskers, potential human health hazards in their handling, and processing difficulties such as deagglomeration, mixing, and settling [10–12]. *In situ*, whisker growth can alleviate these problems. Although, many candidate whisker materials are difficult to grow *in situ*, the formation of elongated, whisker-like grains of β-Si_3N_4 has been observed in multiple studies. In 1973, Lange [13] found that fibrous Si_3N_4 grains could be obtained from a high α-Si_3N_4 content powder. Subsequently, Drew and Lewis [14] observed a large number of elongated β grains in Si_3N_4 containing high concentrations of MgO and impurities. In 1979, Lange [15] reported an improvement in flexural strength and fracture toughness (up to 6 MPa·$m^{1/2}$) when high aspect ratio β-Si_3N_4 grains were formed during sintering. Tani *et al*. [16] obtained elongated Si_3N_4 grains in Si_3N_4-Al_2O_3-Y_2O_3, Si_3N_4-La_2O_3, and Si_3N_4-CeO_2 systems. Pyzik *et al*. [12, 17, 18] developed a Si_3N_4-MgO-Y_2O_3-CaO system reinforced by Si_3N_4 whiskers. The current fracture toughness and flexural strength records published for Si_3N_4 ceramics fall near approximately 9 MPa·$m^{1/2}$ and 1100 MPa respectively [19, 20]. All of these attractive properties, however, were obtained from hot pressed materials, which promotes a high density and a high β-Si_3N_4 content, although at a higher cost.

It has been reported that the main mechanisms responsible for the toughening in Si_3N_4 whisker-reinforced Si_3N_4 ceramics are crack deflection, crack branching, whisker-matrix debonding and to a lesser extent whisker pull-out [20, 21]. An increase in the fracture toughness of these composites with increasing whisker content has also been shown [1, 21]. The studies of the microstructural parameters controlling the fracture behavior show that a high aspect ratio of the reinforced whisker, in combination with a proper size distribution, is an essential requirement of a mechanically

TABLE I Properties of Si_3N_4, BAS and BAS/Si_3N_4 whisker reinforced ceramic

Decomposition temperature of Si_3N_4	1900 °C
Melting temperature of BAS	1760 °C
Theoretical density (g/cm^3):	
α-Si_3N_4	3.168–3.188
β-Si_3N_4	3.190–3.202
BAS	3.260–3.570
Density (Percent of theoretical):	
Dense Si_3N_4	90–100%
Reaction-bonded Si_3N_4	70–88%
BAS/Si_3N_4	95–100%
Coefficient of thermal expansion (20–1000 °C) (10^{-6}/°C):	
Si_3N_4	2.9–3.6
Monoclinic BAS	2.29
Hexagonal BAS	6.6–8.0
Microhardness (Vickers, GPa):	
Si_3N_4	16–20
BAS/Si_3N_4	12
Young's modulus, (RT) (MPa):	
Dense Si_3N_4	300–330
Reaction-bonded Si_3N_4	120–220
BAS	40–50
BAS/Si_3N_4	240–280
Flexure strength (MPa):	
Dense Si_3N_4	500–1100
Reaction-bonded Si_3N_4	150–350
BAS	80–120
BAS/Si_3N_4	520–580
Fracture toughness (MPa·m$^{1/2}$):	
Dense Si_3N_4	4–9
Reaction-bonded Si_3N_4	1.5–2.8
BAS	1.6–2.0
BAS/Si_3N_4	5.2–5.5

reliable ceramic matrix composite [1, 15, 20]. Additionally, it is now widely recognized that the limited high temperature performance of silicon nitride ceramics, including high temperature strength, creep resistance and oxidation resistance, results largely from the presence of residual amorphous phases and/or impurities formed at the grain junctions [1, 2, 22–30]. Four methods are being explored in current research to produce a more refractory material:

(i) The reduction of the fraction of the sintering additive and impurities in the starting composition. This step normally requires compensation by the application of higher pressures.

(ii) The use of sintering additives with high solidus temperatures and high viscosities which tend to form refractory phases.

(iii) Conversion of the amorphous phase to crystalline phases on cooling or during subsequent annealing.

(iv) Selection of a composition where the sintering aids are dissolved in the silicon nitride lattice to form a single-phase system [1].

Barium Aluminum Silicate ($BaAl_2Si_2O_8$), which is referred as "BAS" throughout this paper, has been studied for decades as both in its synthetic form and in its naturally occurring form [31–35]. The polymorphism of stoichiometric BAS at atmospheric pressure is represented graphically in Fig. 1. Below the melting temperature of 1760 °C, BAS exhibits its first solid state phase transformation at 1590 °C, where the stable hexagonal BAS (hexacelsian) transforms into the monoclinic phase, which is stable through room temperature. However, the hexagonal to monoclinic reconstructive transformation is extremely sluggish, causing hexagonal BAS to persist in a metastable state at temperatures below 1590 °C [31, 36]. Upon undercooling, the metastable hexacelsian will transform into an orthorhombic phase at approximately 300 °C. This transformation, which is reversible, is accompanied by about a 3% volume change which is usually destructive [31, 32, 35, 36, 40]. The persistence of hexacelsian phase below 1590 °C, therefore, is generally regarded as an undesirable feature of the BAS ceramic systems.

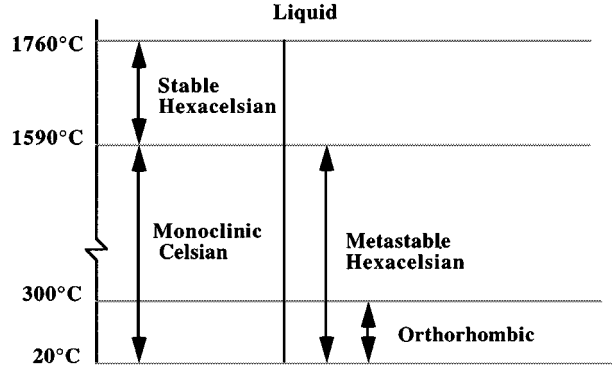

Figure 1 Schematic representation of possible phase transition in the BAS system at atmospheric condition.

Recent work [36–38] has shown that β-Si_3N_4 whiskers could be grown *in situ* from α-Si_3N_4 in the presence of liquid BAS. The presence of the liquid BAS phase is a requirement to assure both the progress of the α to β transformation and the attainment of full pressureless densification.

The unique combination of superior refractory properties (the service temperature for BAS can be as high as 1550 °C and the maximum melting point of celsian BAS is 1760 °C), low density, high modulus, low thermal expansion (celsian's thermal expansion coefficient: 2.29×10^{-6}/°C from 20 to 1000 °C), good oxidation resistance and low dielectric constant, makes the BAS/Si_3N_4 whisker reinforced ceramic composite particularly interesting for high temperature applications [36–38] (see Table I). This ceramic matrix composite exhibits additional advantages of low material cost and relatively low processing costs because near-net-shaped components can be processed to full density at low pressure [36].

Since the microstructure of this material has not yet been well documented, this study is intended to examine the microstructure of this newly developed material by transmission electron microscopy (TEM), high resolution transmission electron microscopy (HRTEM), X-ray diffraction (XRD) and energy dispersive spectroscopy (EDS). This study will examine the interaction between BAS matrix and Si_3N_4, so that future work can identify the mechanisms associated with the mechanical behavior of this composite.

2. Experimental

The BAS/Si_3N_4 composite was manufactured by pressureless sintering of high α-Si_3N_4 powder (<5%β-Si_3N_4 existing in the α-Si_3N_4 starting powder) with BAS constituent powders. The initial 30% BAS, 70% α-Si_3N_4 composition, selected for the present study, corresponds to that optimized for a combination of electromagnetic and mechanical performance [36].

Phase characterization by X-ray diffraction was performed on a Siemens Diffrac-5000 X-ray diffractometer with Ni filtered CuK_α radiation. About 3 grams of ground material were used for each analysis.

The TEM specimens were prepared by diamond cutting, grinding, polishing and ultrasonic cutting, to produce 60 μm thick discs. The resulting disks were then dimpled using standard TEM specimen preparation techniques. The final thinning was accomplished by ion-milling on a cold stage with 4 kV argon ions at incidence angles of 15°, 10° and 8°. The microstructural observations and analyses were carried out in a JEM-2000FX transmission electron microscope fitted with an energy dispersive X-ray spectrometer (EDS). HRTEM images were also obtained to explore the potential presence of amorphous phases.

3. Results and discussion

3.1. X-ray diffraction phase characterization

A typical powder X-ray diffraction spectra of the BAS/Si_3N_4 whisker reinforced ceramic composite is shown in Fig. 2. Three phases were found in this material, including untransformed α-Si_3N_4, β-Si_3N_4, and hexacelsian $BaAl_2Si_2O_8$. Neither orthorhombic BAS nor monoclinic BAS were detected by XRD methods.

To estimate the amount of α-Si_3N_4 phases, the modified XRD intensities of α- and β-silicon nitride (210) diffraction peaks were compared, in a manner described by Gazzara and Messier [41]. From these calculations it was determined that approximately 59% of the initial α-Si_3N_4 had transformed to β-Si_3N_4. Thus, about 40% of the bulk composite is β-Si_3N_4.

3.2. General morphology

The density of the composite, measured by water immersion, was determined to be 3.11 g/cm^3. Using a theoretical density of 3.23 g/cm^3, a relative density of 96% was calculated which compares with that of hot pressed silicon nitride. This indicates that the BAS liquid has enough fluidity to fill the gaps between β-Si_3N_4 whiskers and untransformed α-Si_3N_4 particles during sintering. TEM images of the 70% Si_3N_4-30% BAS composite, shown in Fig. 3, indicate a nearly fully densified material with about 40–45% β-Si_3N_4 whiskers (indicated by "W"), oriented randomly in the fine, nearly continuous matrix of BAS with about 30% of untransformed α-Si_3N_4 grains distributed throughout the material.

The β-Si_3N_4 single crystals, formed from the liquid, are of needlelike morphology with lengths ranging between 30 nm and 4 μm, and aspect ratios between 1.4 and 16.0. About 60% of the whiskers fall within a length dimension of 300 to 700 nm with aspect ratios of 3 to 7. Only a few whiskers (less than 5%)

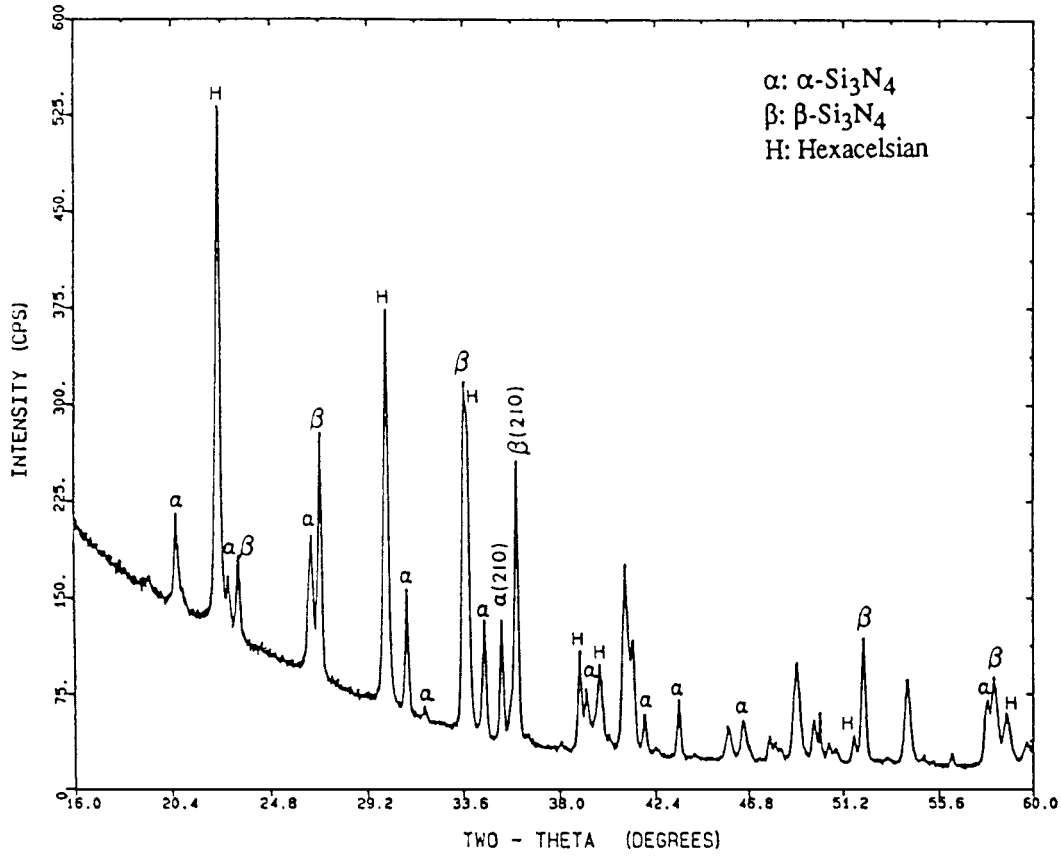

Figure 2 Powder X-ray diffraction spectra of BAS/Si_3N_4 whisker-reinforced ceramic composite.

have lengths over 1 μm. In conventional dense silicon nitride sintered with additives such as MgO, Al_2O_3, and Y_2O_3, whiskers with longer average lengths are obtained but with a significantly smaller aspect ratio [12, 19, 20, 42, 43].

According to Messier *et al*. [44], the α- to β-silicon nitride phase transformation is of a reconstructive nature *via* a solution-reprecipitation mechanism. Nucleation and growth of β-Si_3N_4 grains are a function of the rate of dissolution of α-Si_3N_4 particles, solubility

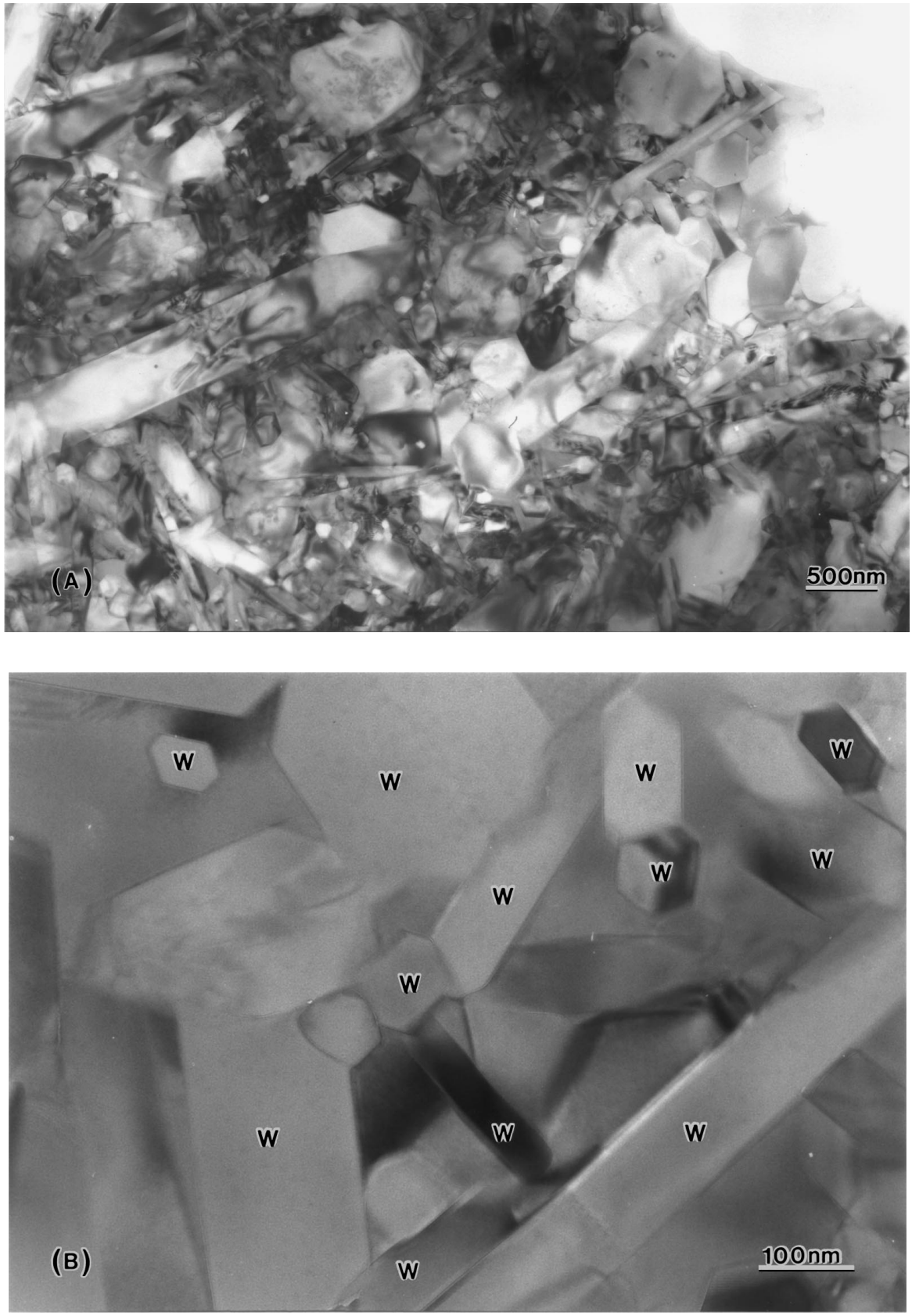

Figure 3 TEM micrograph showing the morphology of BAS/Si_3N_4 whisker-reinforced ceramic composite (Mark "W" indicates the area of Si_3N_4 whiskers) (A) 24,000×, (B) 160,000× and (C) EDS spectra of the Si_3N_4 whiskers. (*Continued*).

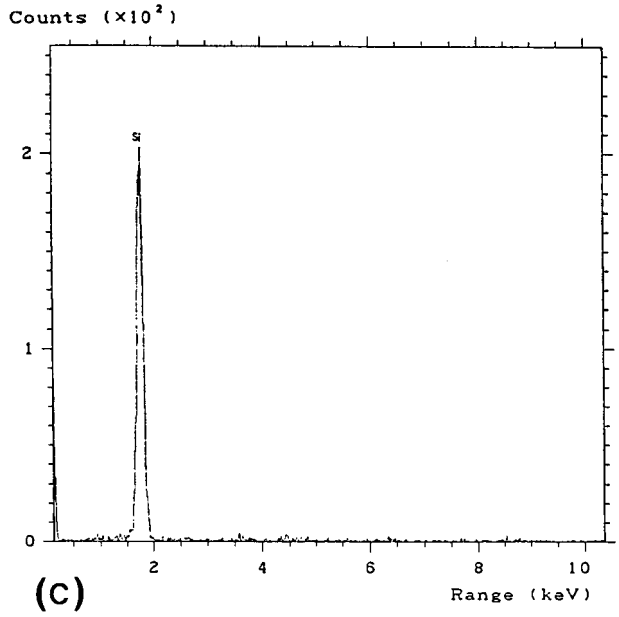

Figure 3 (*Continued*).

of α-Si_3N_4 into the liquid, supersaturation of Si and N in the liquid, interfacial tension and wetting between the silicon nitride grains and liquid, and viscosity of the liquid. The chemistry of the liquid phase is, therefore, a key factor in determining the resulting microstructure and the associated properties of the material.

Although all the BAS (30% of the composite) was a source of liquid phase during sintering, which is much more than the amount of sintering additive normally used in conventional dense silicon nitride, it seems that the large matrix volume does not favor a high rate of α- to β-Si_3N_4 transformation. The melting temperature of BAS is 1760 °C, higher than that of MgO, SiO_2, and CaO, and since the processing temperature is usually less than 100 °C above its melting temperature, the viscosity of liquid phase is expected to remain relatively high during sintering. This high-viscosity liquid phase is expected to inhibit mass transport but increase supersaturation of Si and N during sintering, and therefore causes nucleation of more β whiskers with high aspect ratios [45] and a reduction in the rate of grain growth.

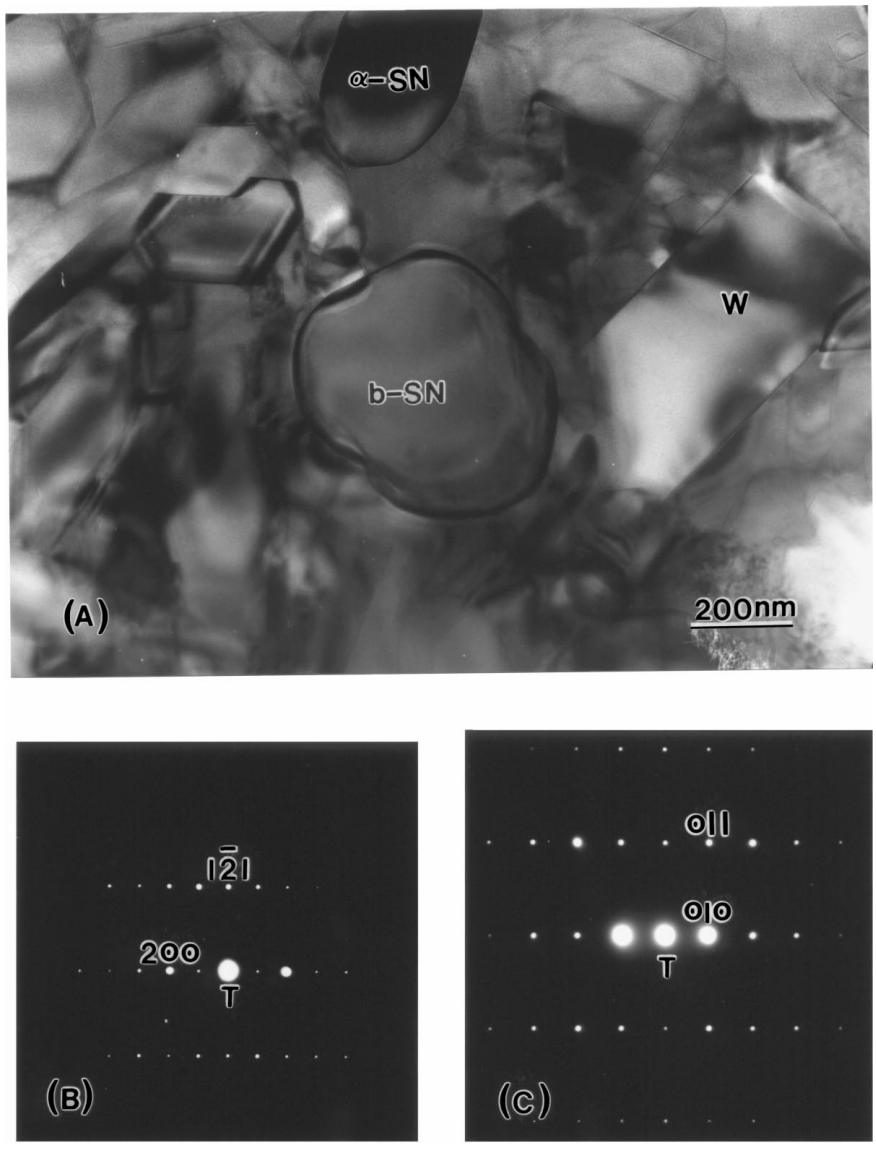

Figure 4 (A) TEM micrograph showing the morphology of equiaxed β-Si_3N_4 (marked b-SN), (B) $[\bar{1}2\bar{1}6]$ electron diffraction pattern of the equiaxed β-Si_3N_4 and (C) $[1\bar{2}16]$ electron diffraction pattern of the equiaxed β-Si_3N_4.

These conditions promoted whiskers of short and thin morphology.

β-Si_3N_4 has an extensive solid solubility with Al_2O_3 [1, 4]. Significant dissolution of Al_2O_3 into β-Si_3N_4 may shift the composition of BAS away from the stoichiometric composition. This may increase the amount of residual glass phase. EDS analysis of the whisker areas revealed no substitution of silicon or nitrogen in the Si_3N_4 structure by metal ions (Fig. 3C). This indicates no Si-Al-O-N composition was formed during processing.

Although some dislocation features could be observed in some of the larger whiskers, the authors believe that this may have resulted from electron bombardment. These features appear to be associated with the bending of the large whiskers due to localized heating during TEM observation. Dislocation networks, which may appear in the *in situ* formed silicon nitride whiskers processed under hot-pressing, were not observed [21].

Equiaxed β-Si_3N_4 grains with diameters of several hundred nanometers were also observed in this material (see Fig. 4). Since both α- and β-Si_3N_4 have a hexagonal structure, with nearly equal *a*-axis parameters, but the *c*-parameter of α-Si_3N_4 is about twice as large as that for the β-Si_3N_4 [1], the difference of electron diffraction patterns between α and β is not very significant. Several diffraction patterns were used to confirm the identity of the equiaxed areas shown. Fig. 4B and C are electron diffraction patterns of $[1\bar{2}16]$ and $[2\bar{1}\bar{1}0]$ directions, respectively, taken from the equiaxed β-Si_3N_4 grain (marked "b-SN" in Fig. 4A). The EDS results suggest that the chemical composition also matches that of the whiskers (β-Si_3N_4). Although β-Si_3N_4 whiskers tend to grow equiaxed if the sintering time is excessively long, the morphology of the grain shown in Fig. 4A seems different from equiaxed morphologies resulting from long sintering times. The appearance of this kind of equiaxed β-Si_3N_4 grains indicates they may have a different nucleation and growth mechanism from β-Si_3N_4 whiskers. Mitomo *et al*. [43, 44] showed that both α-phase Si_3N_4 and whiskerlike β-Si_3N_4 starting powders can result in elongated grain morphology following processing. This finding indicates that the

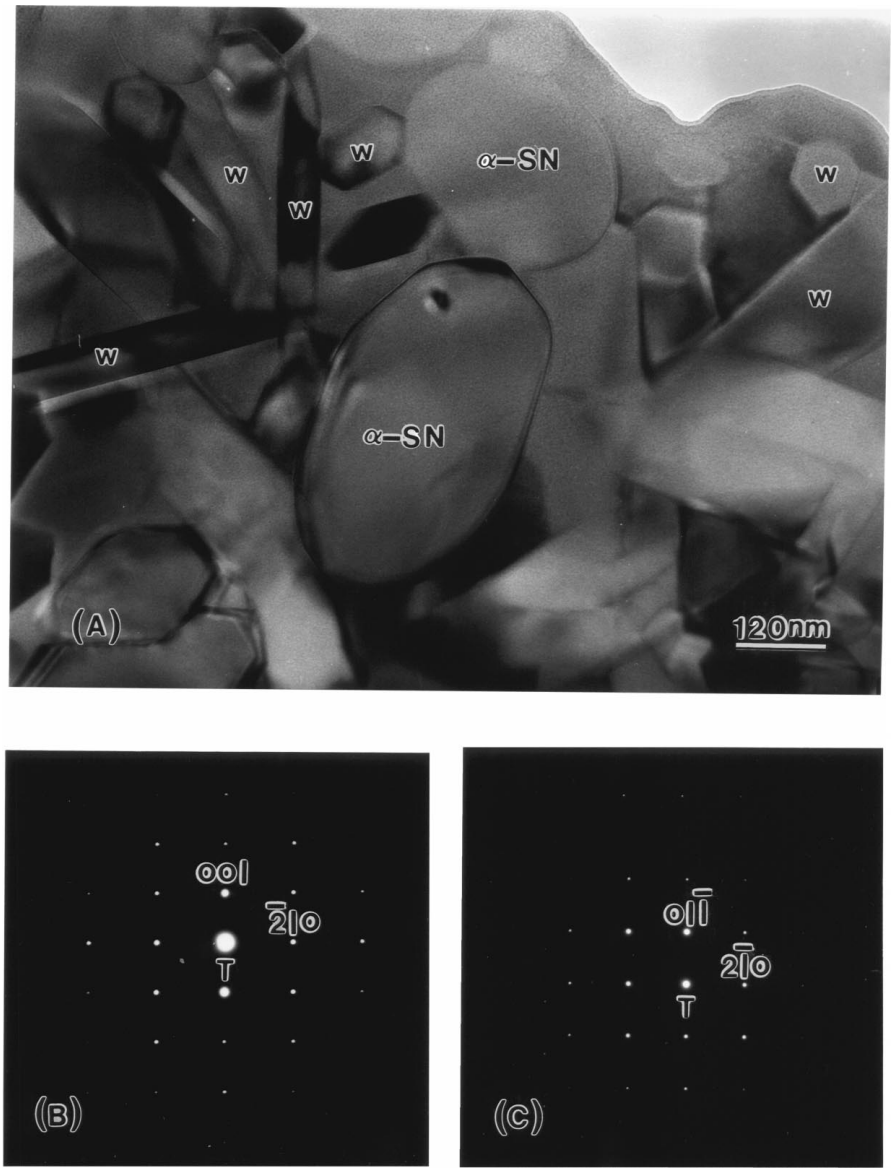

Figure 5 (A) TEM micrograph showing the morphology of α-Si_3N_4 (marked "α-SN"), (B) $[01\bar{1}0]$ electron diffraction pattern of the α-Si_3N_4 and (C) [0112] electron diffraction pattern of the α-Si_3N_4.

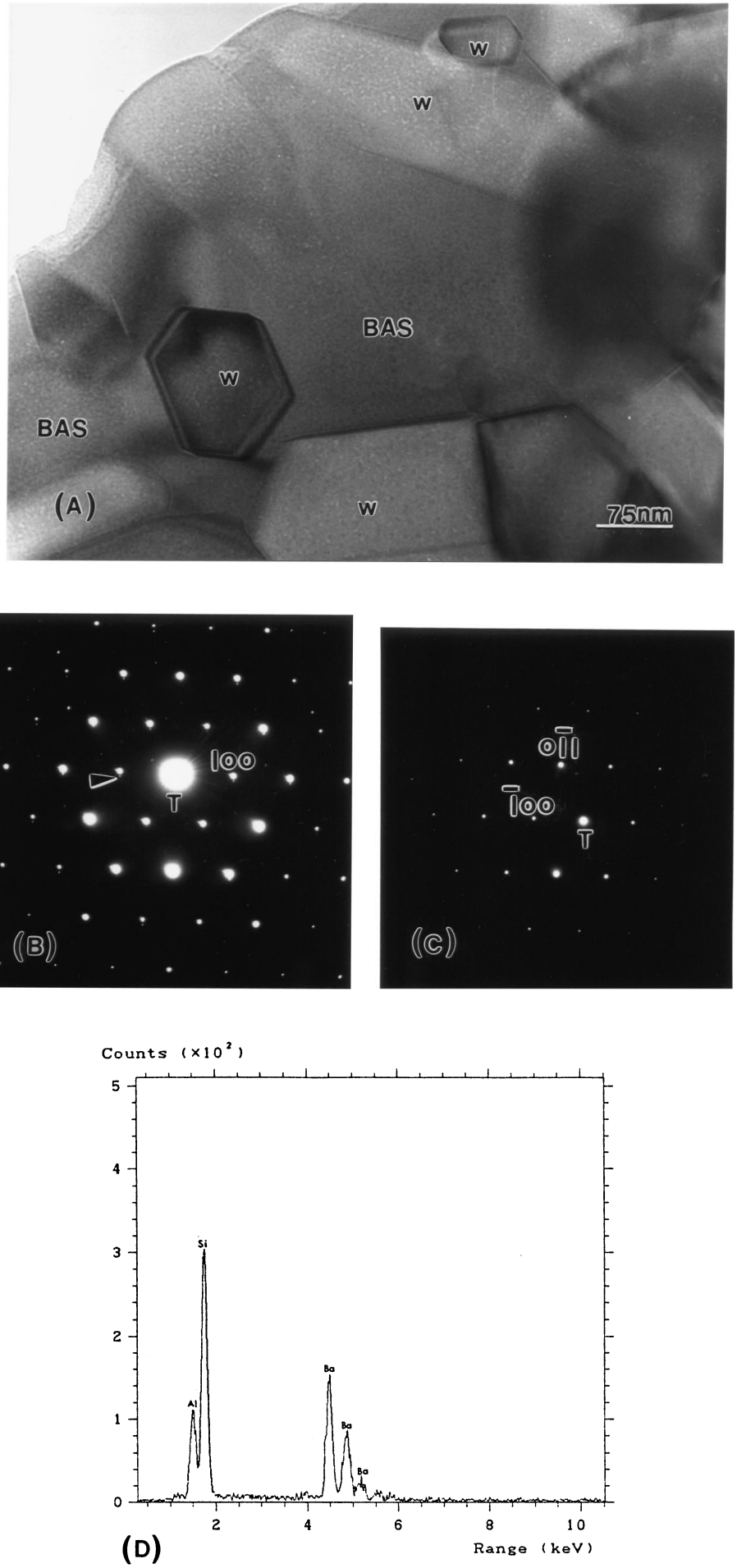

Figure 6 (A) TEM micrograph showing the morphology of hexagonal BAS (marked "BAS"), (B) [0001] electron diffraction pattern of the BAS, (C) [1$\bar{2}\bar{1}$3] electron diffraction pattern of the BAS and (D) EDS spectra of the BAS.

equiaxed β-phase grains can not be obtained from re-precipitation from the liquid or directly nucleated at the newly formed β-Si_3N_4 elongated grain surface. However, according to Lange [13, 15] and Lee *et al*. [46], the sintering of equiaxed β starting powder, produces a microstructure consisting of large equiaxed grains, resulting in relatively low mechanical properties. Therefore, a possible interpretation for the appearance of equiaxed β grains in this composite is that these grains grow from the small amount (about 5%) of β-Si_3N_4 powders, which exist in the starting compact.

Residual α-Si_3N_4 observed in the sintered material indicates that the α-β phase transformation is not complete (Fig. 5A). The residual α-Si_3N_4 grains

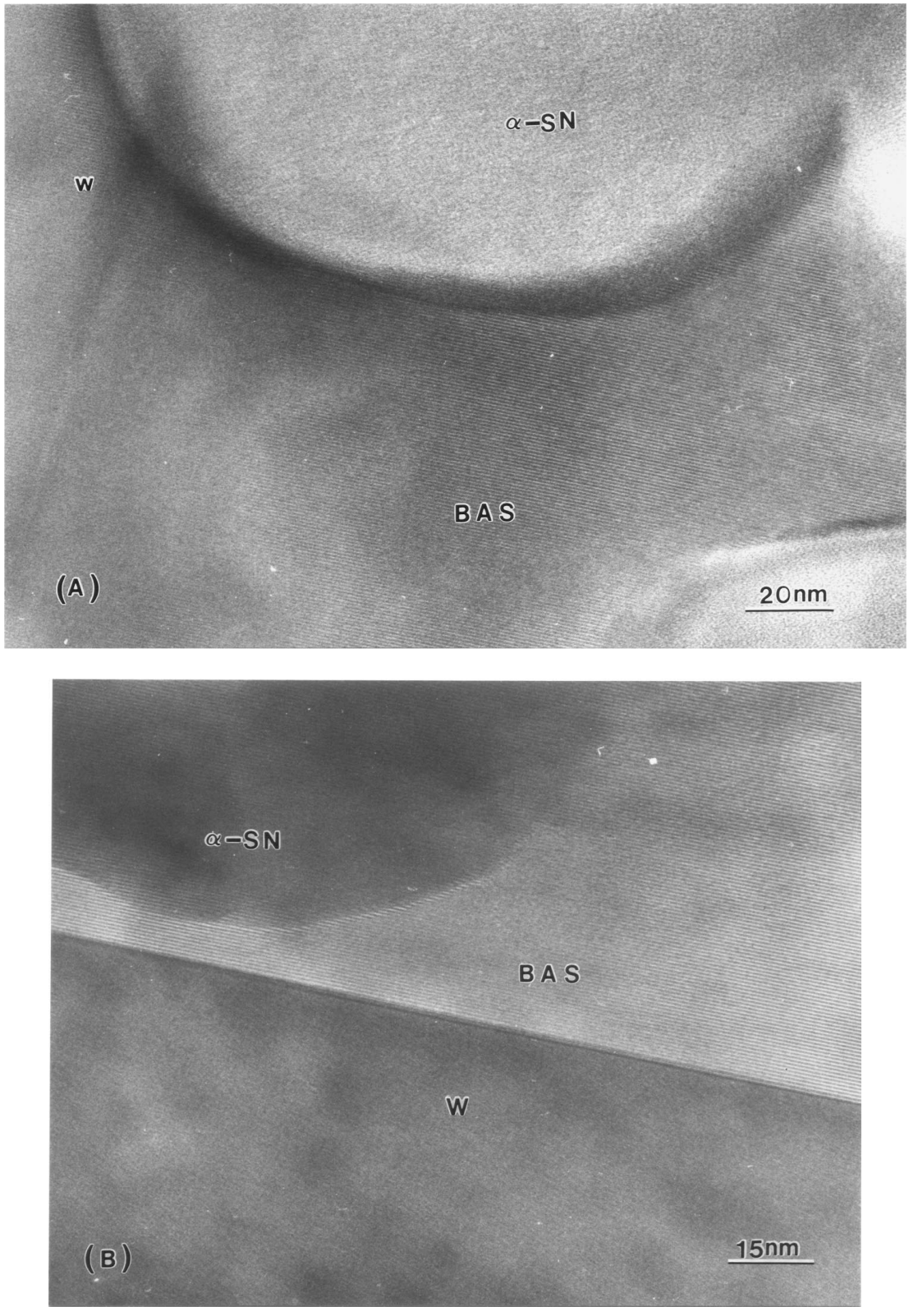

Figure 7 HRTEM micrograph showing (A) the crystallization of BAS matrix (marked "BAS") among α-Si_3N_4 (marked "α-SN") and β-Si_3N_4 (marked "W") grains, (B) the crystallization of BAS matrix between α-Si_3N_4 and β-Si_3N_4 whisker, (C) $[5\bar{1}43]$ electron diffraction pattern of the BAS area in (B) and (D) EDS spectra of the BAS area in (B).

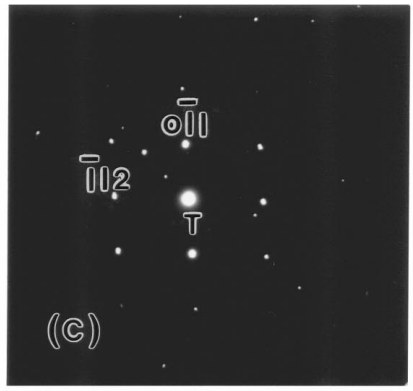

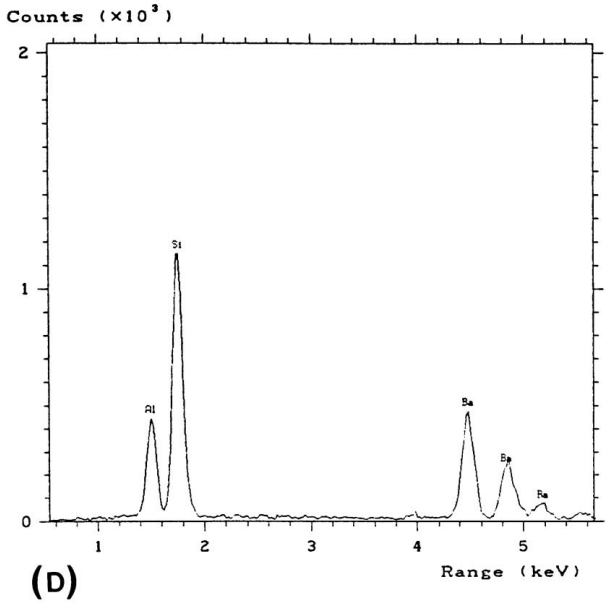

Figure 7 (*Continued*).

observations showed dimensions ranging from 200 nm to 1 μm. Fig. 5B and C are the electron diffraction patterns of [0110] and [01$\bar{1}$2] directions respectively, of the residual α-Si_3N_4 area marked "α-SN" in Fig. 5A. This amount of residual α-Si_3N_4 suggest that the dissolution of α-Si_3N_4 starting particles into the liquid and the mass transport capability of the liquid phase are limited under current processing conditions.

3.3. The crystallization of BAS and residual glass phase

In this material, the BAS glass-ceramic serves not only as a liquid phase sintering aid for the α-β silicon nitride phase transformation, but also remains as a structural matrix. Volume fractions as high as 30% were used, in contrast to the amounts of sintering additives normally added to conventional Si_3N_4 ceramics, which is usually under 10%. We expect that these large quantities of BAS will more strongly influence the composite properties than would sintering additives.

Compared with other silicate glasses the BAS glass is extremely refractory, with a dilatometric softening point of 925 °C [32]. However, for high temperature applications, it is necessary to crystallize the glass to the highly refractory BAS crystalline phase.

From Fig. 6A, the BAS matrix appears to be virtually continuous. Since the size of BAS pockets are no larger than 1 μm, structure determination by both electron diffraction and EDS analysis were employed to characterize this phase. The [0001] (Fig. 6B) and [1213] (Fig. 6C) electron diffraction patterns of the area marked "BAS" in Fig. 6A confirms the hexagonal structure, with c/a ratio of 1.493 (hexacelsian). This agrees with several studies of monolithic BAS [47, 48]. The extra weak reflections, indicated by arrows in Fig. 6B, suggest ordering of the Al and Si atoms in the BAS. EDS also confirms that the BAS composition is $BaAl_2Si_2O_8$.

In this composite, no celsian was detected by either electron diffraction or XRD methods. Apparently, the sluggish kinetics of hexacelsian to monoclinic celsian phase transformation was sufficiently suppressed to preclude the appearance of the celsian.

In monolithic BAS, the high-temperature polymorph, hexacelsian, undergoes a rapid, reversible transformation at 300 °C from the hexagonal to an orthorhombic structure and is accompanied by a volume change of 3% or greater. Takeuchi [47] studied this phase transformation in monolithic BAS by X-ray diffraction and found that it only requires small changes in oxygen atom positions. Thus, as stated by Takeuchi [47] "No significant differences are observed between the powder XRD patterns of the orthorhombic and hexagonal hexacelsian except peak shifts owing to lattice expansion, indicating that the fundamental frameworks of both structures are the same." Neither electron diffraction nor X-ray diffraction, therefore, are effective methods to detect this transformation in the composite, if the hexagonal and orthorhombic phases are to be distinguished. Therefore, the present studies were unable to exclude the presence of orthorhombic BAS. However, recent dilatometry studies of similar compositions by Bandyopadhyay *et al*. [40] identified the potential existence of this transformation in the BAS/Si_3N_4 composite, showing that the magnitude of the volume change decreased with increasing amount of Si_3N_4. For the 70%Si_3N_4-30%BAS composite, the dilatometric indication of transformation is only 1/5 of that for the 30%Si_3N_4-70%BAS composite. A drop in the transformation temperature was also found with an increase in the β-Si_3N_4 content in the composite. Although, no detailed study was conducted here, the BAS phase transition to the stable orthorhombic phase appears to have been restricted by the presence of Si_3N_4 grains in the 70%Si_3N_4-30%BAS composite. Since monoclinic celsian is stable at all temperatures below 1500 °C, alternative processing methods which promote the hexacelsian to celsian phase transition would avoid this mechanically destructive transition.

The use of materials at higher temperatures requires not only a refractory matrix composition, but also a microstructure which does not soften due to the presence of grain boundary glassy phases. The activation energy for crystallization of BAS glass, measured by Bansal and Hyatt [32] as 558 kJ/mol for bulk BAS glass, predicts relatively easy crystallization behavior. The nearly complete crystallization of BAS matrix, shown in Fig. 7A and B, supports this prediction and

illustrates an important advantage of this composite for higher temperature applications. The hexacelsian always nucleates homogeneously from the glass phase because it has a simpler structure of higher symmetry, compared with that of celsian. The hexagonal forms are roughly built of alternative double sheets of Si-N tetrahedron and a single layer of Ba^{2+} cations normal to the *C*-axis [34, 48]. In contrast, the low symmetry form, celsian [34] consists of three dimensional networks in which the Al and Si are at least partially ordered. Due to these structure differences, the high symmetry forms, such as hexacelsian, have lower kinetic barriers for nucleation, and therefore tend to dominate the microstructure.

In monolithic BAS, some uncrystallized glass phase may remain along the grain boundaries if the processing time is insufficient. In this composite, since the space between α- and β-silicon nitride grains is quite small, usually less than 1 μm, and the processing time and temperature is sufficient for extensive crystallization, these intergranular pockets usually contain a single grain of hexagonal BAS which has consumed other small grains (Fig. 7A and B). As shown in Fig. 8A and C, several BAS grains were also observed within one pocket. However, these grains tend to be in contact with each other with a more thermodynamically stable interface, such as a low angle grain boundary. Thus, the glass-ceramic BAS may be entirely crystallized by controlled processing so as to eliminate any residual amorphous phase between BAS grains.

Using HRTEM methods, some glass phase was found at the triple-grain junction of α/β silicon nitride and BAS grains (Fig 9). Areas such as these are assumed to be residual from an incomplete crystallization of BAS. In grain boundaries between α/β Si_3N_4 grains, both situations, with and without glass layer, were observed (Fig. 10A and B), perhaps suggesting the dominance of a different growth mechanism for local Si_3N_4 whiskers. As the β-Si_3N_4 whiskers nucleate and grow from the

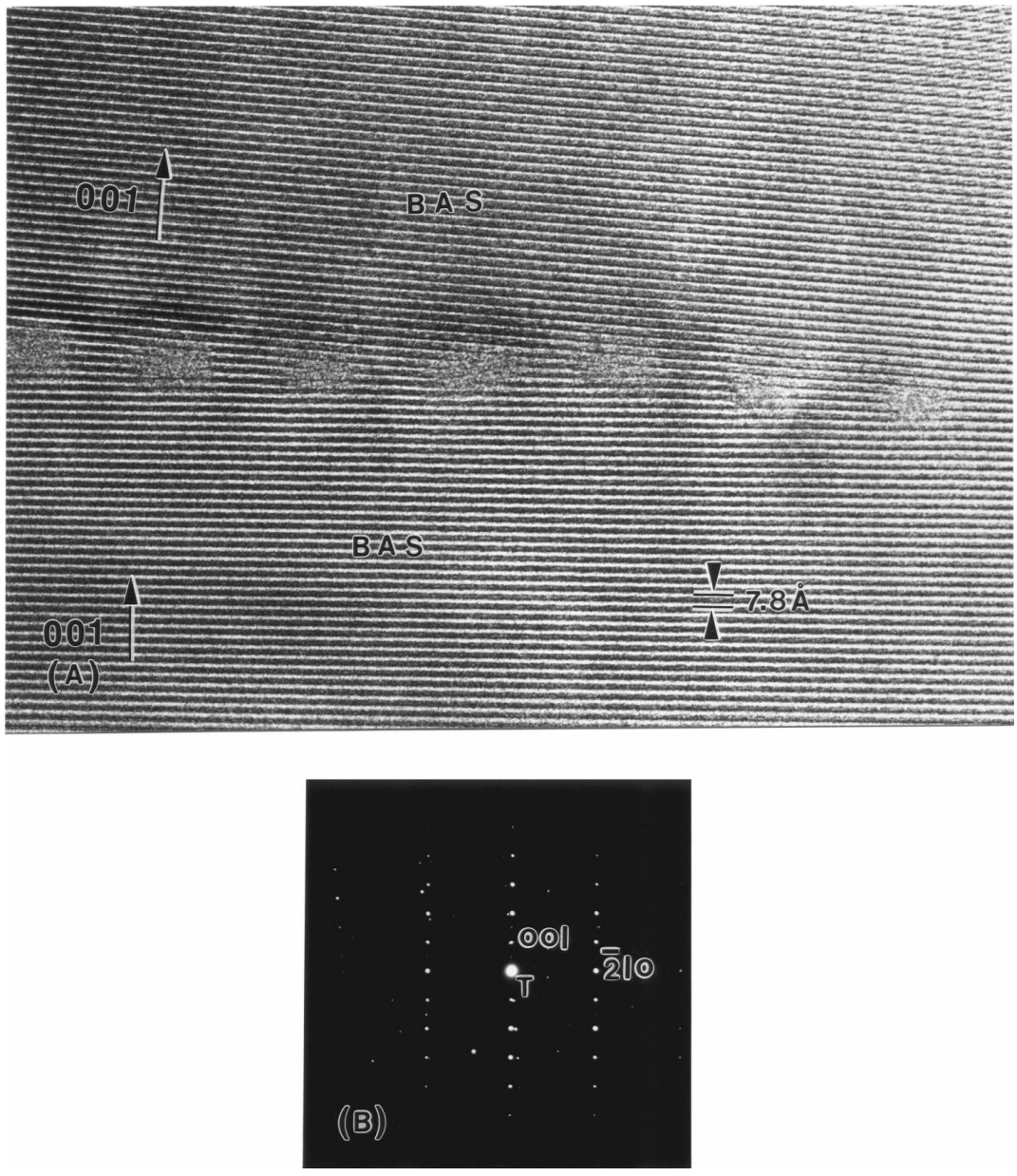

Figure 8 HRTEM images of grain boundaries in BAS matrix: (A) low-angle grain boundary between two BAS grains, (B) $[01\bar{1}0]$ electron diffraction pattern of BAS taken from the grain boundary area and (C) triple junction of three BAS grains.

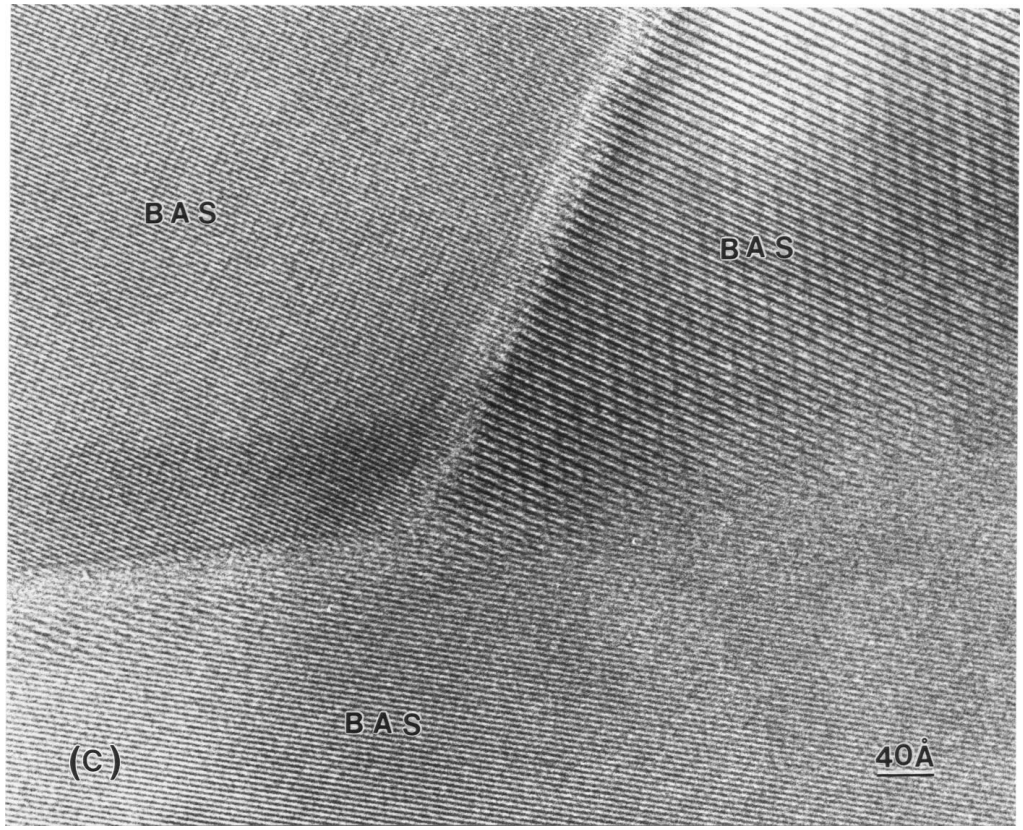

Figure 8 (*Continued*).

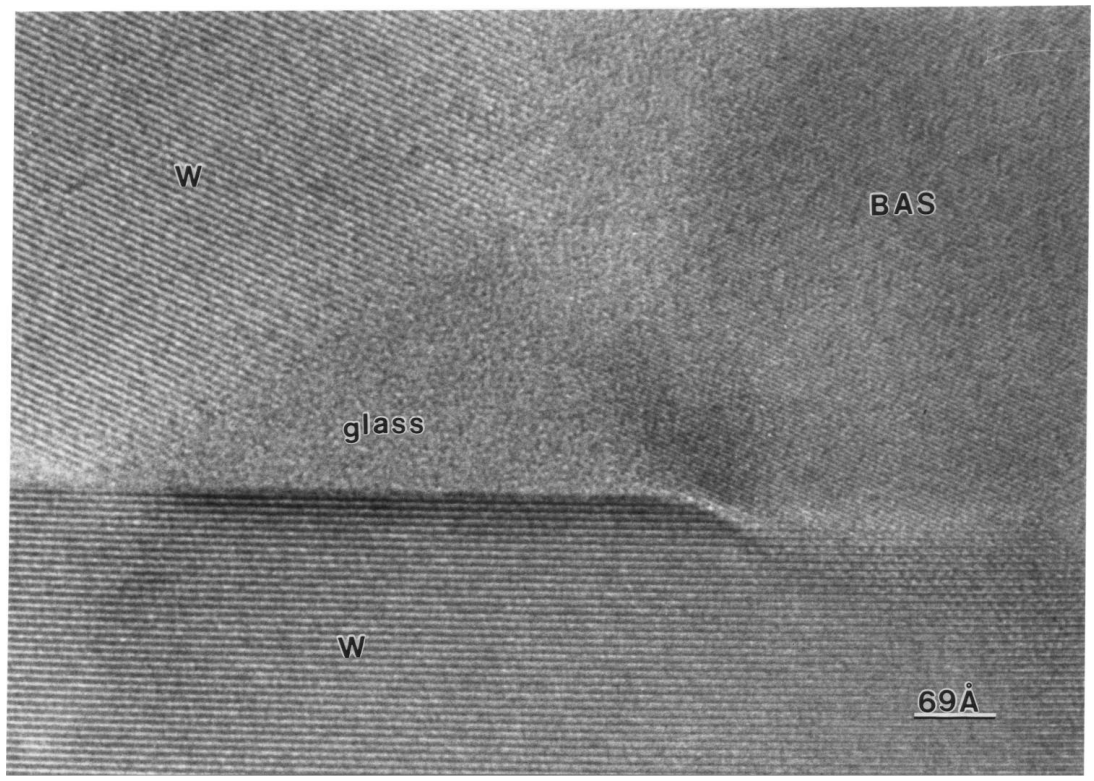

Figure 9 HRTEM image of triple junction of grains showing the existence of glass pocket.

liquid phase, the surfaces approach one another or those of residual α-Si_3N_4 grains, causing a decrease in thickness of the intergranular phase until an equilibrium value is attained [49, 50], as shown in Figs 10B and 11. Since a significant amount of α-Si_3N_4 remains after the transformation, the former interface type is quite common in this composite. The smallest thickness of the interlayer between α/β Si_3N_4 measured by HRTEM in a manner described by Kirvanek *et al*. [51] and Cinibulk *et al*. [52] is about 1 nm (Fig. 10B). But it is also possible that a β-Si_3N_4 whisker could nucleate heterogeneously at an α-Si_3N_4 grain surface if the nucleation

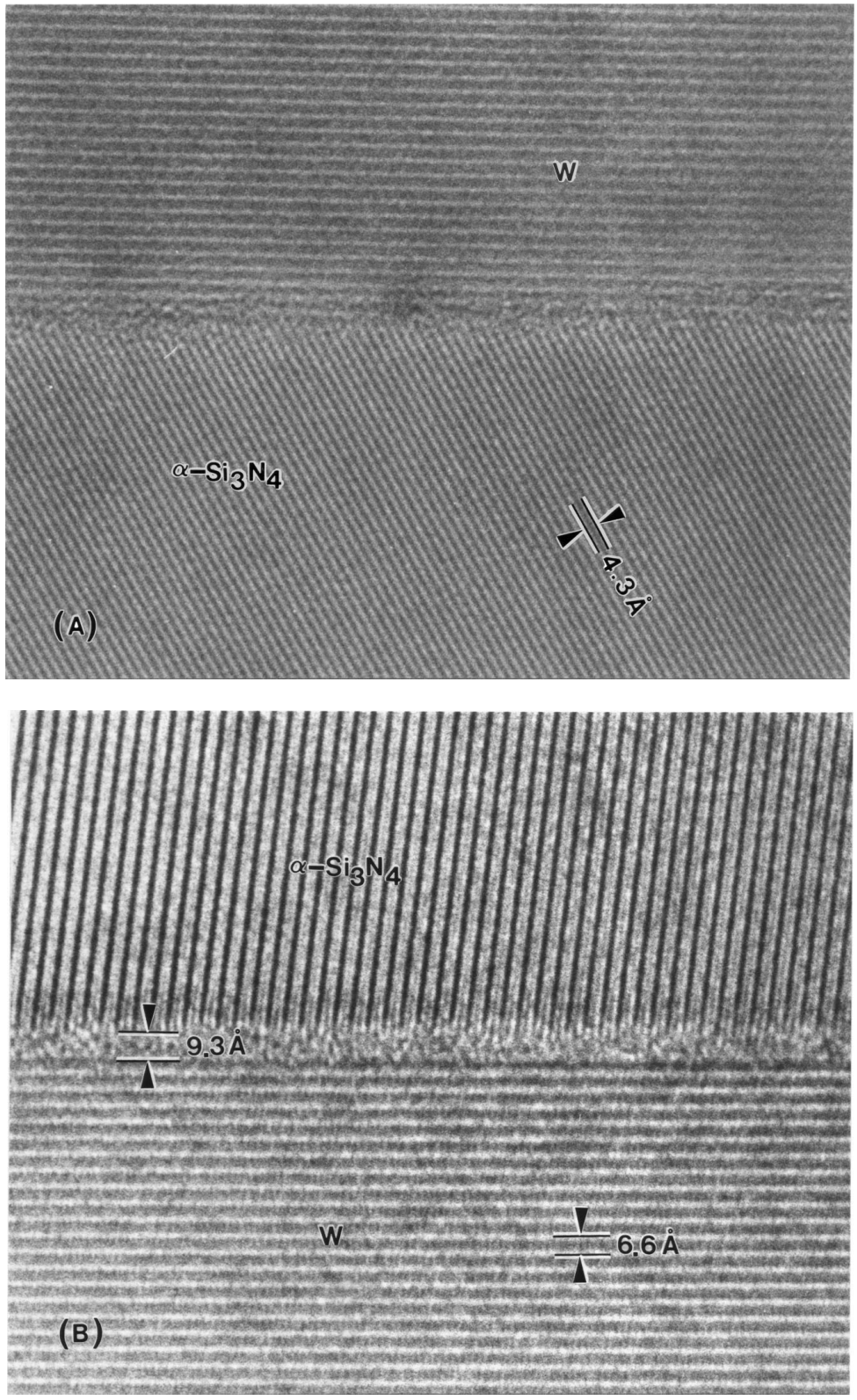

Figure 10 HRTEM images of interfaces between α- and β-Si_3N_4 grains: (A) showing no glass phase existing, (B) the existence of glass phase.

requirements are met. This may explain the population of clean α/β Si_3N_4 grain boundaries found in the microstructure (Fig. 10A).

An interlayer of glass phase of about 1 nm thick was observed between α/β Si_3N_4 whiskers, as shown in Fig. 11. From theoretical calculations [49, 50, 53], this thin layer is theoretically stable and the energy barrier to dewetting is considerably larger than thermal activation for any realistic values of a dewetting force. This implies that homogeneous nucleation of dewetting is nearly impossible, thus requiring some form of heterogeneous nucleation.

3.4. Observation of crack path

SEM and TEM observations implicate crack deflection, crack branching, whisker-matrix debonding and, to a lesser extent, whisker pull-out, as principle toughening

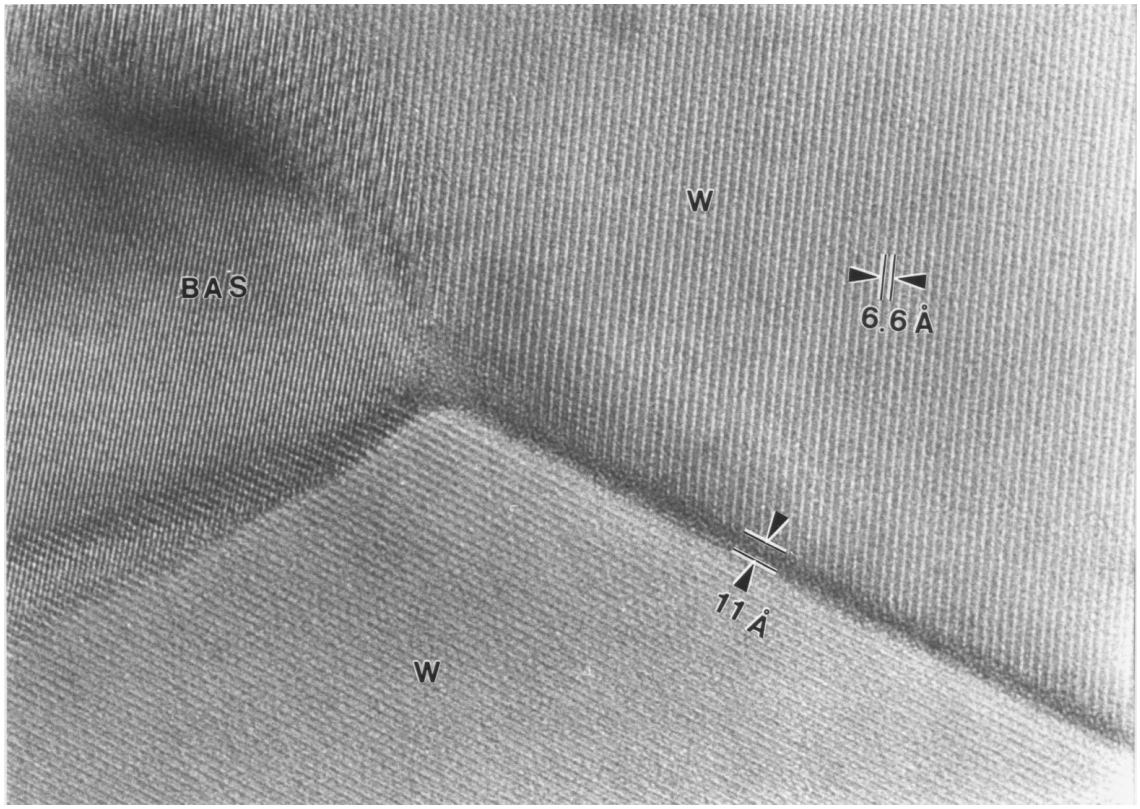

Figure 11 HRTEM image of triple junction between two β-Si_3N_4 whiskers and a BAS grain.

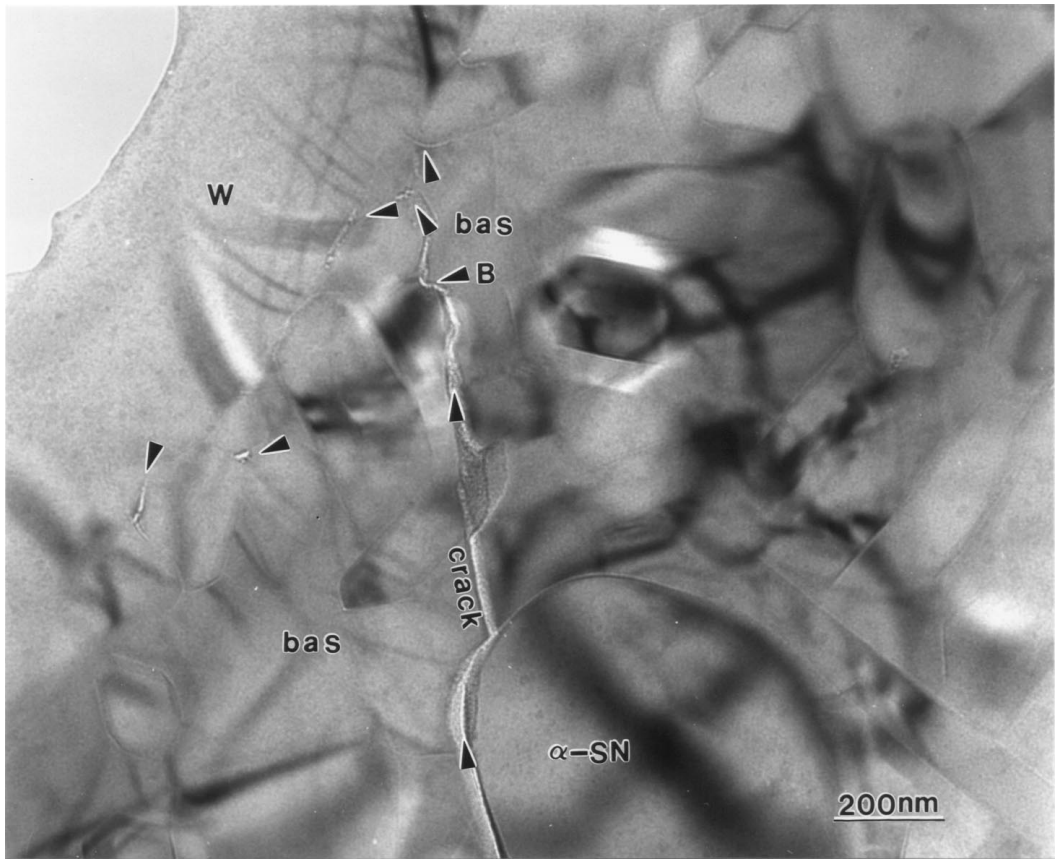

Figure 12 (A) TEM observations reveal that cracks could be deflected and arrested by whisker in the BAS/Si_3N_4 composite and (B) image of enlarged area marked "B" in (A).

mechanisms. The crack of Fig. 12A which was taken from a peninsulalike sample area, apparently induced by localized heating during TEM observation, follows a growth path along the whisker interface which shows contrast indications of dislocations and residual strain fields. It seems that the heating of this specimen has an effect of bending this area towards the whisker. Also crack branching and whisker-matrix

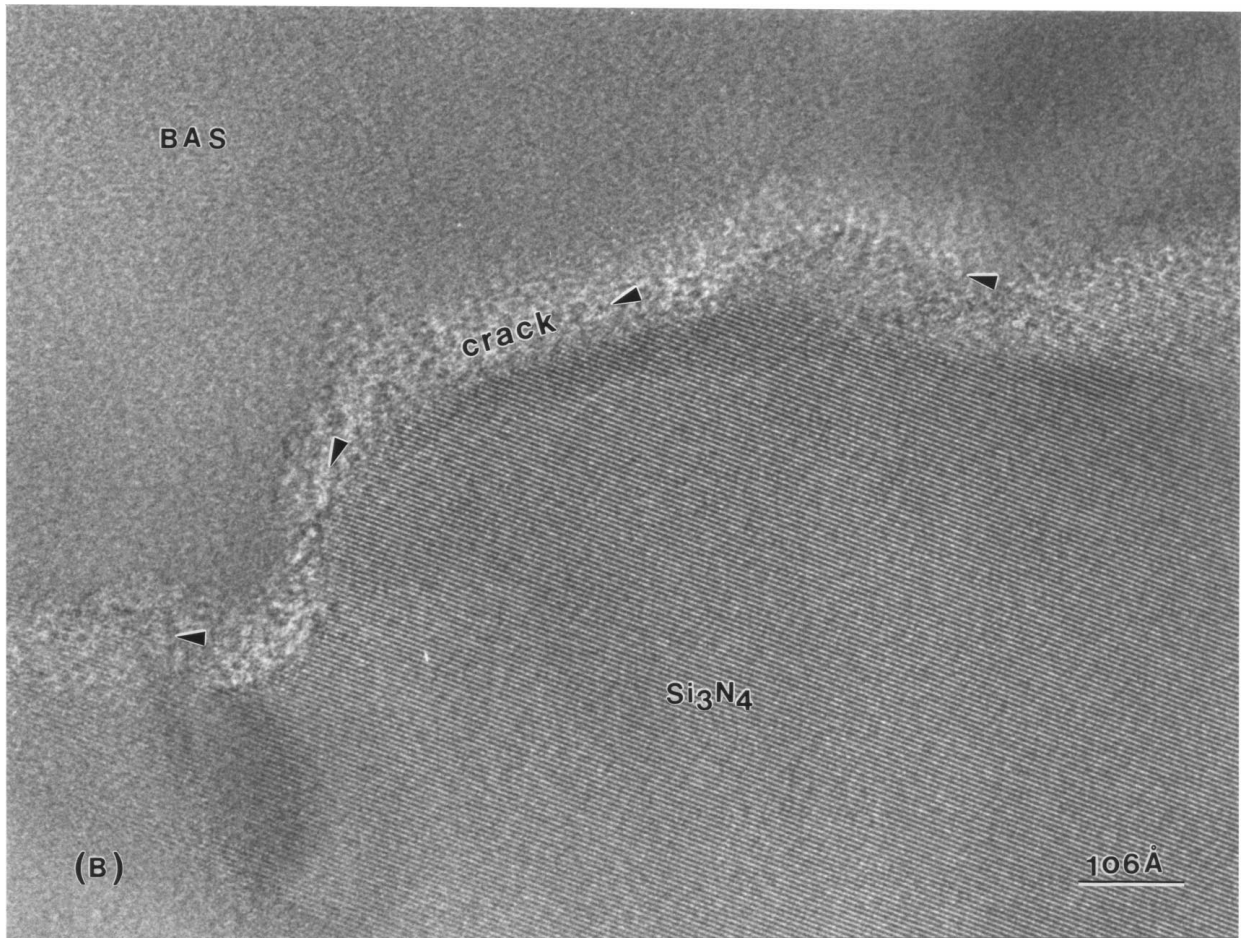

Figure 12 (*Continued*).

interface debonding are evident. In either case, the development of interface debonding allows the matrix crack to proceed without fracturing the whisker. Fig. 12A also suggests that the variation of interface integrity contributes to a tortuous crack path.

TEM observations reveal that most of the crack path follows the grain boundaries between BAS grains and either α-Si_3N_4 or β-Si_3N_4 grain, rarely through a BAS pocket. Fig. 12B is an enlarged image of area marked "B" in (A). The areas of Si_3N_4 and BAS were identified by EDS respectively. Lattice fringes in the Si_3N_4 area confirm the absence of grain boundaries, while the grain boundary between Si_3N_4 and BAS matrix is clearly shown. The crack path was labeled in Fig. 12B. This implies that the BAS pockets consist of single BAS grains, or that any grain boundaries existing in these areas are of high crack growth resistance.

4. Conclusion

BAS is a promising matrix material for Si_3N_4 whiskers. β-Si_3N_4 whiskers nucleate and grow in random directions in the nearly continuous matrix of hexacelsian BAS. These results find the BAS matrix to be nearly completely crystallized as metastable hexacelsian. Although small amounts of amorphous phase remains in some grains junctions, the configuration of the interface between whiskers appears to approach thermodynamic stability, suggesting little opportunity for improved crystallization of the grain boundary glass between whiskers. Residual α-Si_3N_4 and equiaxed β-Si_3N_4 grains which are distributed among the whiskers, may degrade the mechanical properties and therefore warrant further study.

Acknowledgements

The authors wish to thank Loral Vought Systems, Dallas, TX, for providing the material. Also, gratitude is extended to Ms. Vicky Milonopoulou, Chemical Engineering Department, University of Houston, for her help in the XRD experiments, Mr. Zheng Xu for providing mechanical property data of this composite, and the assistance from Dr's. J. Kulic and I. Rusakova in TEM study. This work was supported, in part, by Texas Coordinating Board Grant Number 003652123-ATP.

References

1. G. ZIEGLER, J. HEINRICH and G. WÖTTING, *J. Mater. Sci.* **22** (1987) 3041.
2. R. RAJ, *J. Amer. Ceram. Soc.* **76**(9) (1993) 2147.
3. F. F. LANGE, *Int'l Metals Rev.* **1** (1980) 1.
4. J. WEISS, *Ann. Rev. Mater. Sci.* **11** (1981) 381.
5. G. H. CAMPBELL, M. RUHLE, B. J. DALGLEISH and A. G. EVANS, *J. Amer. Ceram. Soc.* **73**(3) (1990) 521.
6. P. F. BECHER, C. HSUEH, P. ANGELINI and T. N. TIEGS, *ibid.* **71**(12) (1988) 1050.
7. G. PEZZOTTI, I. TANAKA and T. OKAMOTA, *ibid.* **74**(2) (1991) 326.

8. T. OHJI, Y. GOTO and A. TSUGE, *ibid*. **74**(4) (1991) 739.
9. T. OHJI and Y. YAMAUCHI, *ibid*. **76**(12) (1993) 3105.
10. J. D. BIRCHALL, D. R. STANLY, M. J. MOCKFORD, G. H. PIGOTT and P. J. PINTO, *J. Mater. Sci. Letters* **7** (1989) 350.
11. G. E. WEI and P. F. BEEKER, *Ceram. Bull*. **64**(2) (1985) 298.
12. A. J. PYZIK and D. R. BEAMAN, *J. Amer. Ceram. Soc*. **76**(11) (1993) 2737.
13. F. F. LANGE, *ibid*. **56** (1973) 518.
14. P. DREW and M. H. LEWIS, *J. Mater. Sci*. **9** (1974) 261.
15. F. F. LANGE, *J. Amer. Ceram. Soc*. **62**(7/8) (1979) 428.
16. E. TANI, S. UMEBAYASHI, K. KISHI, K. KOBAYASHI and M. NISHIJIMA, *Amer. Ceram. Soc. Bull*. **65**(9) (1986) 1311.
17. A. J. PYZIK, W. J. DUBENSKY, D. B. SCHWARZ and D. R. BEAMAN, US Pat. no. 4883776 (1989).
18. A. J. PYZIK, D. B. SCHWARZ, W. J. DUBENSKY and D. R. BEAMAN, US Pat. no. 4919689 (1990).
19. M. J. HOFFMANN, *MRS Bull*. **10**(2) (1995) 28.
20. P. F. BECHER, S. HWANG and C. HSUEH, *ibid*. **10**(2) (1995) 23.
21. J. DUSZA, D. SAJGALIK and M. REECE, *J. Mater. Sci*. **26** (1991) 6782.
22. D. R. CLARKE and G. THOMAS, *J. Amer. Ceram. Soc*. **60**(11/12) (1977) 491.
23. L. K. V. LOU, T. E. MITCHELL and A. H. HEUER, *ibid*. **61**(9) (1978) 392.
24. C. C. AHN and G. THOMAS, *ibid*. **66**(1) (1983) 14.
25. M. K. CINIBULK, H. KLEEBE, GEROLD A. SCHNEIDER and M. RUHLE, *ibid*. **76**(11) (1993) 2801.
26. I. TANAKA, H. KLEEBE, M. K. CINIBULK, J. BRULEY, D. R. CLARKE and M. RUHLE, *ibid*. **77**(4) (1994) 911.
27. R. L. TSAI and R. RAJ, *ibid*. **63**(9/10) (1980) 513.
28. M. N. MENON, H. T. FANG and D. C. WU, *ibid*. **77**(5) (1994) 1217.
29. S. H. KNICKEROCKER, A. ZANGVIL and S. D. BROWN, *ibid*. **68**(4) (1985) C-99.
30. C. CHU, J. P. SINGH and J. ROUTBORT, *ibid*. **76**(5) (1993) 1349.
31. H. C. LIN and W. R. FOSTER, *The American Mineralogist* **53** (1968) 134.
32. N. P. BANSAL and M. J. HYATT, *J. Mater. Res*. **4**(5) (1989) 1257.
33. A. K. IVUKINA and Y. I. PANOVA, *Soviet Physics-Crystallography* **9**(4) (1965) 473.
34. T. ITO, "X-ray Studies on Polymorphism" (Maruzen Co. Ltd., Tokyo, 1950) p. 19.
35. C. H. DRUMMOND III and N. P. BANSAL, *Ceram. Eng. Sci. Proc*. **11**(7/8) (1990) 1072.
36. D. BAHAT, *J. Mater. Sci*. **5** (1970) 805.
37. C. H. DRUMMOND III, *J. of Non-Crystalline Solids* **123** (1990) 114.
38. A. BANDYOPADHYAY, S. W. QUANDER, P. ASWATH, D. W. FREITAG, K. K. RICHARDSON and D. L. HUNN, "Metallurgica of Materialia," in press.
39. D. W. FREITAG and K. K. RICHARDSON, Private communication.
40. A. BANDYOPADHYAY, P. B. ASWARTH, W. D. PORTER and O. B. CAVIN, *J. Mater. Res*., in press.
41. C. P. GAZZARA and D. R. MESSIER, *Amer. Ceram. Soc. Bull*. **56**(9) (1977) 777.
42. M. MITOMO, M. TSUTSUMI and H. TANAKA, *J. Amer. Ceram. Soc*. **73**(8) (1990) 2441.
43. M. MITOMO and S. VENOSONO, *ibid*. **75**(1) (1992) 103.
44. D. R. MESSIER, F. L. RILEY and R. J. BROOK, *J. Mater. Sci*. **13** (1978) 1199.
45. G. WÖTTING, B. KANKA and G. ZIEGLER, "Non-Oxide Technical and Engineering Ceramics" (Elsevier Applied Science, London, England, 1986) p. 83.
46. D. LEE, S. L. KANG, G. PETZOW and D. N. YOON, *J. Amer. Ceram. Soc*. **73**(3) (1990) 767.
47. Y. TAKEUCHI, *Mineralogical Journal* **2**(5) (1958) 311.
48. B. YOSHIKI and K. MATSUMOTO, *J. Amer. Ceram. Soc*. **34** (9) (1951) 283.
49. D. R. CLARKE, *ibid*. **70**(1) (1987) 15.
50. R. RAJ, *ibid*. **64**(5) (1981) 245.
51. O. L. KIRVANEK, T. M. SHAW and G. THOMAS, *J. Appl. Phys*. **50**(6) (1979) 4223.
52. M. CINIBULK, H. KLEEBE and M. RÜHLE, *J. Amer. Ceram. Soc*. **76**(2) (1993) 426.
53. D. R. CLARKE, "Surface and Interfaces of Ceramic Materials" (Kluwer Academic Publishers, New York, 1989) p. 57.

Received 28 July
and accepted 23 December 1998